



HAL
open science

Precessional changes in the western equatorial Pacific Hydroclimate: A 240 kyr marine record from the Halmahera Sea, East Indonesia

Haowen Dang, Zhimin Jian, Catherine Kissel, Franck Bassinot

► **To cite this version:**

Haowen Dang, Zhimin Jian, Catherine Kissel, Franck Bassinot. Precessional changes in the western equatorial Pacific Hydroclimate: A 240 kyr marine record from the Halmahera Sea, East Indonesia. *Geochemistry, Geophysics, Geosystems*, 2015, 16 (1), pp.148-164. 10.1002/2014GC005550 . hal-01806666

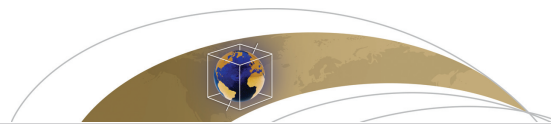
HAL Id: hal-01806666

<https://hal.science/hal-01806666>

Submitted on 9 Oct 2020

HAL is a multi-disciplinary open access archive for the deposit and dissemination of scientific research documents, whether they are published or not. The documents may come from teaching and research institutions in France or abroad, or from public or private research centers.

L'archive ouverte pluridisciplinaire **HAL**, est destinée au dépôt et à la diffusion de documents scientifiques de niveau recherche, publiés ou non, émanant des établissements d'enseignement et de recherche français ou étrangers, des laboratoires publics ou privés.



RESEARCH ARTICLE

10.1002/2014GC005550

Key Points:

- The age model is established with reliability on precession band
- The provenance of sediment is determined to be mainly locally derived
- The terrigenous fraction varies in-phase with boreal autumn insolation

Supporting Information:

- Readme
- Supplementary Figures
- Table S1
- Table S2
- Table S3

Correspondence to:

H. Dang,
hwdang@gmail.com

Citation:

Dang, H., Z. Jian, C. Kissel, and F. Bassinot (2015), Precessional changes in the western equatorial Pacific Hydroclimate: A 240 kyr marine record from the Halmahera Sea, East Indonesia, *Geochem. Geophys. Geosyst.*, 16, 148–164, doi:10.1002/2014GC005550.

Received 19 AUG 2014

Accepted 21 DEC 2014

Accepted article online 29 DEC 2014

Published online 20 JAN 2015

Precessional changes in the western equatorial Pacific Hydroclimate: A 240 kyr marine record from the Halmahera Sea, East Indonesia

Haowen Dang¹, Zhimin Jian¹, Catherine Kissel², and Franck Bassinot²

¹State Key Laboratory of Marine Geology, Tongji University, Shanghai, China, ²Laboratoire des Sciences du Climat et de l'Environnement/IPSL, CEA—CNRS—UVSQ, Gif-sur-Yvette, France

Abstract Within the precession band, an interhemispheric antiphase pattern in the tropical hydroclimate is supported by many paleorecords, and optimally explained by the forcing of precessional insolation change. However, scenarios within the western equatorial Pacific (WEP), which plays the role of the ascending center of atmospheric convection, remain poorly determined. In this study, a marine sediment core from the Halmahera Sea, East Indonesia, was analyzed with high-resolution XRF scanning, quantitative discrete XRF, and ICP-AES/MS measurements. The terrigenous fractions in this core are constrained by their trace elemental characteristics to be locally sourced from Halmahera Island, and hence reflect variations in the local riverine runoff and precipitation. On this basis, a continuous record of precipitation changes of the western equatorial Pacific was reconstructed with multidecadal resolution over the last ~240 ka, using an age model established by the correlation between an adjusted ice volume model and benthic $\delta^{18}\text{O}$ constrained by ^{14}C dating. The records of terrigenous input show a dominant ~23 kyr periodicity with a $90^\circ\sim 100^\circ$ phase lag to the boreal summer (i.e., in-phase with the boreal autumn) insolation change. This pattern can be explained by the variability in the convective activity over the WEP, which might be primarily controlled by precessional changes in the El Niño and Southern Oscillation (ENSO) system. A dynamic linkage is implied between the precessional variations in the convective activity in the WEP and the East Asian and Australia-Indonesian summer monsoons (EASM and AISM), in the sense of their distinct stable phase relationship to precession.

1. Introduction

On orbital time scales, a primary control by precession on variations in the tropical hydroclimate is now largely accepted, and is best explained by a conceptual hypothesis involving a direct forcing of the interhemispheric antiphase summer insolation on the latitudinal migration of the Intertropical Convergence Zone (ITCZ) and the monsoonal rainfall belt [e.g., *Haug et al.*, 2001; *Kutzbach et al.*, 2008]. Findings in stalagmite $\delta^{18}\text{O}$ records from both hemispheres convincingly support this hypothesis [*Wang et al.*, 2001, 2008; *Yuan et al.*, 2004; *Cruz et al.*, 2005; *Wang et al.*, 2007; *Liu et al.*, 2014]. One remaining prominent debate concerns the phase relationships between the insolation forcing and the tropical hydrology, particularly when the distant transport of moisture and latent heat [e.g., *Kutzbach et al.*, 2008; *Ruddiman*, 2006; *Clemens and Prell*, 2007] and the land-ocean contrast of heat capacity [*Clement et al.*, 2004; *Kutzbach et al.*, 2008] are considered.

Key information for addressing such issues may lie in the Indo-Pacific Warm Pool (IPWP), which is a major source of atmospheric convective activities on Earth and hence critical for the global hydroclimate. Within the IPWP, the regional precipitation is seasonally associated with the latitudinal migration of the ITCZ and the summer monsoon bands (EASM and AISM) [*Hamada et al.*, 2002; *Aldrian and Susanto*, 2003; *Chang et al.*, 2005; *Moron et al.*, 2008, 2010], and interannually modulated by the zonal displacement of the convection center associated with ENSO [*Lau and Nath*, 2000; *Hamada et al.*, 2002; *Aldrian and Susanto*, 2003; *Wang*, 2003; *Hung et al.*, 2004]. The orbital-scale variations in these seasonal and interannual processes are of great interest for a better understanding of the tropical hydroclimate.

Previous reports of terrigenous input from the southern hemisphere areas of the IPWP generally show dominant precessional variations in-phase with austral summer (December to February) insolation change, and

have been proposed to be controlled by the AISM [Lückge *et al.*, 2009; Tachikawa *et al.*, 2011; Wu *et al.*, 2012, 2013]. These findings are supported by the stalagmite $\delta^{18}\text{O}$ record from Flores Island [Griffiths *et al.*, 2009] and are consistent with the hemispheric summer insolation forcing hypothesis. However, uncertainties still exist. One major contrasting view comes from northern Borneo stalagmite $\delta^{18}\text{O}$ records, which can be largely explained by the impact of September–October insolation on the regional convective activities [Partin *et al.*, 2007; Carolin *et al.*, 2013]. Records of modern tree-ring $\delta^{18}\text{O}$ from Cambodia [Zhu *et al.*, 2012], Holocene records of leaf wax δD from Sulawesi [Tierney *et al.*, 2012], and stalagmite $\delta^{18}\text{O}$ from northern Australia [Denniston *et al.*, 2013] also highlight the significance of the September–October–November (SON) season and the influences of ENSO and the Indian Ocean Dipole on the IPWP hydroclimate.

Either originating from the Pacific or the Indian Ocean, changes in the rising limb of the Walker Circulation are the major driving force of the hydroclimate of the WEP. The impact of ENSO-related changes on the drought/humid conditions over the IPWP have been documented by records of pollen assemblage and charcoal content [van der Kaars and Dam, 1995; Beaufort *et al.*, 2003; van der Kaars *et al.*, 2006, 2010; Kershaw *et al.*, 2007]. However, these records do not provide a continuous record of variability in the atmospheric convection over the IPWP. To date, our understanding of the dynamics of the IPWP's hydroclimate on orbital time scales has been hindered by the lack of continuous records of the hydroclimatic response of the WEP to insolation change.

In this study, a high-resolution reconstruction of terrigenous input from the Halmahera Sea is presented, providing a high-quality continuous record of local precipitation variability of the WEP. By comparison to other well-dated regional precipitation archives, insights are provided into orbital-scale changes in the convective activity in the WEP and its relation with the monsoons.

2. Geologic and Climatic Background of Halmahera Region

The Halmahera region, characterized by the K-shaped Halmahera Island, occupies a critical position in the western Equatorial Pacific and eastern Indonesian Archipelago at the junction of the Eurasia, Indo-Australia, and Philippine Sea Plates [e.g., Ballantyne, 1991]. It has formed since the late Cretaceous by subductions beneath the Halmahera Subplate of the Philippine Sea Plate from the east and the Molucca Sea Plate from the west and north [Hall *et al.*, 1988]. As a result, the basement rocks of Halmahera are characterized by mantle-derived ophiolites in the east, and volcanic and volcanoclastic deposits in the west [Hall *et al.*, 1988, 1991; Ballantyne, 1991], covered by Cretaceous–Eocene and Mio-Pliocene clastic and carbonate sedimentary rocks [Hall *et al.*, 1988; Hakim and Hall, 1991] (Figure 1c).

Because of the small size of the islands, there are only small rivers that drain the islands of the Halmahera region (Figure 1b). Direct investigations about these specific rivers is scarce, but the fluvial sediment discharge of these rivers is estimated to be very large because of the sharp gradients of elevation (Figure 1b) [Milliman and Farnsworth, 2011]. The Halmahera Sea is a quasi-confined marginal basin embraced by the southeast and southwest branches of Halmahera Island with a maximal water depth of ~ 2000 m (Figure 1b) and much shallower sills linking to the Pacific Ocean at the northeast (< 1000 m) and to the Ceram Sea at the southwest (< 500 m). As a major entrance portal where South Pacific waters feed into the Indonesian Throughflow [Gordon, 2005], the Halmahera Sea is characterized by waters partly derived from the New Guinea Coastal Undercurrent (NGCUC) [Cresswell and Luick, 2001]. Based on mooring observations in 1993–1994, the annual mean current above 700 m in Halmahera Sea is ~ 1.5 Sv southward, mainly driven by the NW monsoon. During the SE monsoon season, the shallow current (~ 400 m) can be reversed to the northwestward [Cresswell and Luick, 2001].

The precipitation over the Halmahera region is generally abundant throughout the year [Hamada *et al.*, 2002] and shows a weak semiannual cycle with relatively more rainfall during January to June (Figure 1d) [Aldrian *et al.*, 2004; Chang *et al.*, 2005]. This semiannual pattern was suggested to be related to the semiannual changes in local convection [Aldrian and Susanto, 2003], controlled by seasonal changes in local SST due to switches of the source of surface water in the Halmahera and Molucca Seas [Godfrey, 1996; Morey *et al.*, 1999]. A few sites in this region show either a weak rainfall peak in June–July [Aldrian and Susanto, 2003], or biannual rainfall peaks related to the twice-a-year crossing of the Sun over the equator [Chang *et al.*, 2005]. Besides the Halmahera and Molucca region (Figure 1a, domain C), seasonal precipitation patterns over other parts of the IPWP are either concentrated in November–March as controlled by the AISM (domain A) or show biannual peaks (October–November and March–May) associated with the twice-a-year crossing of the ITCZ (domain B), as defined by Aldrian and Susanto [2003] (Figure 1a).

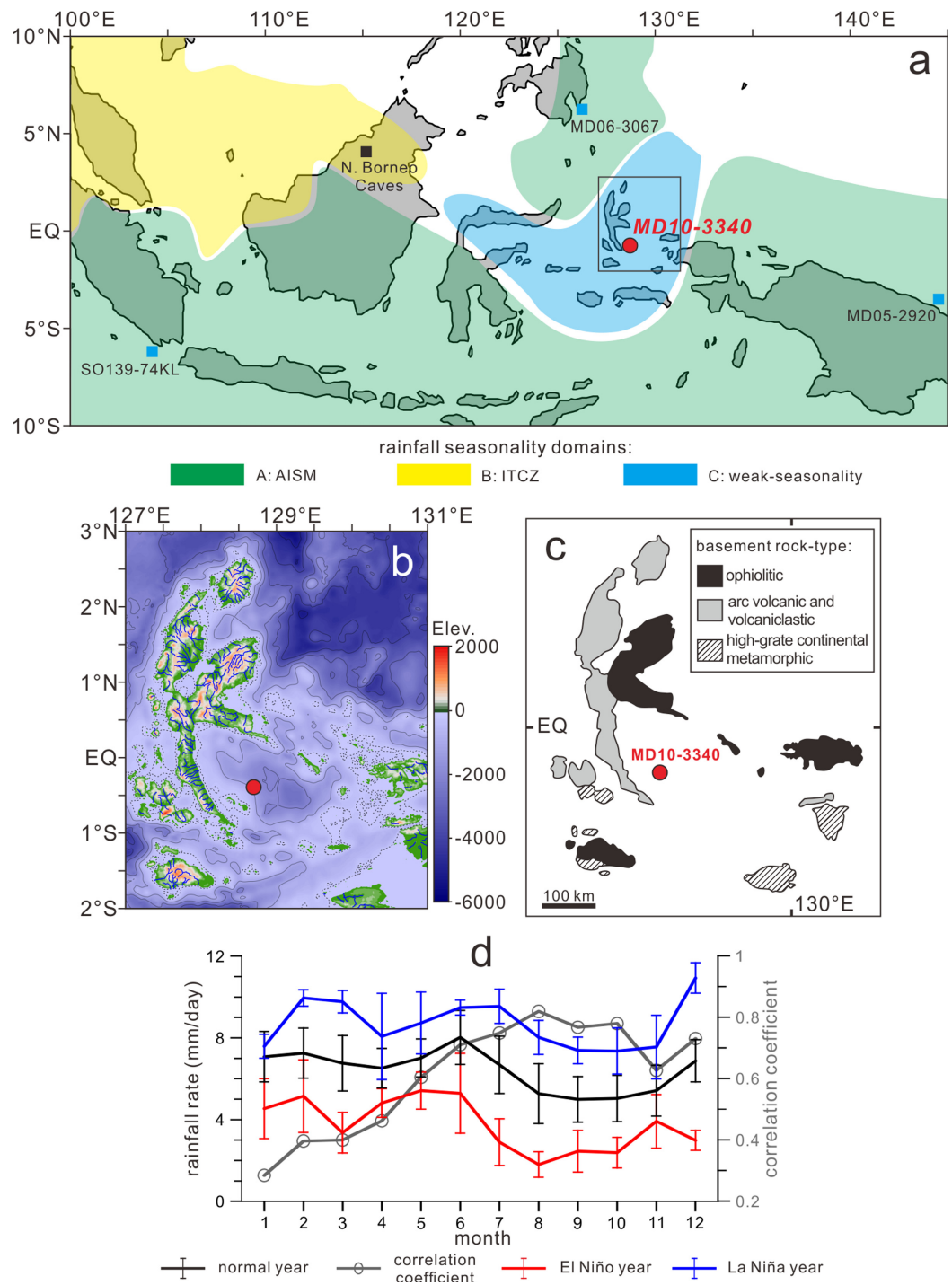


Figure 1. Geology and Climate background of Halmahera. (a) A regional view of the IPWP region with the domains of seasonal precipitation pattern (transparent shadings, modified from Aldrian and Susanto [2003]), sites of MD10–3340 and previous published precipitation records are indicated. (b) Bathymetry of Halmahera region, elevation shown in color shading and the contour interval (solid line) is 1000 m, 100 m water depth shown in dotted line. (c) Basement rocks of the Halmahera region. (d) Monthly rainfall over the Halmahera region (127–129°E, 2.5°N–1.5°S, 1979–2008) in normal (black), El Niño (red), and La Niña (blue) years (error bars: 1σ), and the Pearson correlation coefficient (gray) between annual mean and monthly precipitation rates from 1979 to 2014. Red solid circles in Figures 1b and 1c show the site of MD10–3340. Bathymetry data from SRTM30 (<http://srtm.csi.cgiar.org>), rainfall data from GPCP2.2 [Adler et al., 2003].

The annual mean rainfall over Halmahera is strongly correlated to the monthly rainfall of the later half-year from July to December ($r=0.74 \pm 0.06$) (Figure 1d, monthly rainfall data from GPCP2.2, 1979–2014) [Adler et al., 2003]. This means that on the interannual and longer time scales, the regional annual mean rainfall

amount is greatly determined by the season from July to December. A direct explanation involves the inter-annual oscillations associated with ENSO, which always peaks in the later half-year [Rasmusson and Carpenter, 1982; Philander, 1983]. Precipitation over the Halmahera region is intensively enhanced during La Niña and dampened during El Niño (Figure 1) and negatively correlated with the Niño3 SST index [Aldrian and Susanto, 2003]. In addition, precipitation over Halmahera also shows positive correlations to the SST over the western Pacific and South Pacific Convergence Zone, indicating the influence of the Walker Circulation [Aldrian and Susanto, 2003].

3. Materials and Method

Core MD10-3340 (00°30.98'S, 128°43.47'E, water depth 1094 m, total core length of 34.10 m) was retrieved with a giant CALYPSO piston corer during the MD181 MONOCIR cruise in 2010 on board the French R.V. *Marion Dufresne* (Figure 1). MD10-3340 sediments consist of homogeneous fossiliferous gray clays without any apparent disturbance. After XRF core scanning, the core was subsampled at 1 cm intervals, and the top 10 cm were combined as one subsample since it was suprahedrous and mixed during coring. Subsamples of every 2–4 cm were wet washed and sieved (0.063 mm mesh size) to obtain the coarser fraction ($>63 \mu\text{m}$), mainly foraminifera. All the analyses except for the AMS ^{14}C dating were conducted in the State Key Laboratory of Marine Geology, Tongji University.

High-resolution, nondestructive elemental analyses were performed on the sediment surface of the core at 0.5 cm steps with an Avaatech XRF (X-ray fluorescence) Core Scanner (detailed procedure see Wu *et al.* [2013]). Semiquantitative elemental measurements were conducted at settings of 10, 30, and 50 kV with 30 s of counting time, and reported as counts per second. The results are reported as “[element]_scan” hereafter. The Cl intensity was used to monitor and correct the attenuation effect of water content [Tjallingii *et al.*, 2007; Hennekam and de Lange, 2012] on lighter elements from Al to Ca.

The quantitative chemical composition of bulk sediment was determined for every 20 cm interval by conventional XRF, and for selected subsamples from every MIS stage by ICP-AES and ICP-MS (Inductive Coupled Plasma-Atomic Emission Spectroscopy and Mass Spectroscopy). Therefore, the CaCO_3 fraction is counted into the total Ca concentration (in other words, the CaCO_3 concentration shown in this work is converted from CaO by multiplying by 100/56). Prior to discrete XRF analysis, $>6 \text{ g}$ bulk sediment was ground to $<74 \mu\text{m}$. A total of $>4.5 \text{ g}$ was then pressed into a sample bead (4 cm diameter, 0.7 cm thick, bottom filled with boric acid) for XRF measurements on trace elements, and $0.70000 \pm 0.00008 \text{ g}$ was melted with $7.0000 \pm 0.0008 \text{ g}$ of fusion agent (mixture of lithium tetraborate and lithium metaborate) into a sample bead (3.7 cm diameter, 0.7 cm thick) for measurements on major elements and for eliminating possible influences derived from grain size and mineral grain. The prepared sample beads were measured on a PANalytical AXIOSmAX, with a standard RSD of $<2\%$ based on replicate analyses of GSR6, GSS14, and GSD15 standards.

For ICP-AES/MS analysis, $>1 \text{ g}$ bulk sediment was ground and heated in a 600°C Muffle furnace for 2 h, and then $>45 \text{ mg}$ was totally digested by ultrapure acid (1:1 HNO_3 and pure HF). The 1000 times elution of these sample solutions (with ultrapure 2% HNO_3) were analyzed by an ICP-AES (IRIS Advantage) for major elements, and 10,000 times elution analyzed by an ICP-MS (Thermo VG-X7 mass spectrometer) for trace elements, with an average RSD of $<6\%$ based on replicate analyses of GSR5, GSR6, and GSR9 standards.

Stable oxygen and carbon isotopes were measured on a MAT252/253 stable isotope ratio mass spectrometer on 133 samples of benthic foraminiferas (mainly *Uvigerina peregrina* and occasionally mixed with *U. auberiana*) from selected intervals (roughly every 1 kyr), with a standard uncertainty of 0.07% on $\delta^{18}\text{O}$ [Cheng *et al.*, 2005]. AMS ^{14}C dates were performed on 10 samples of *Globigerinoides ruber* s.s. white ($8.45 \pm 2.20 \text{ mg}$) by BETA Analytic, USA.

4. Results

4.1. Chronostratigraphy of Core MD10-3340

The age model for core MD10-3340 is based on AMS ^{14}C dating and benthic $\delta^{18}\text{O}$ stratigraphy. The obtained ^{14}C ages were converted into calendar ages using a regional reservoir age of 309 years (estimated by the model of Butzin *et al.* [2005], <http://radiocarbon.LDEO.columbia.edu>), and the Fairbanks0107

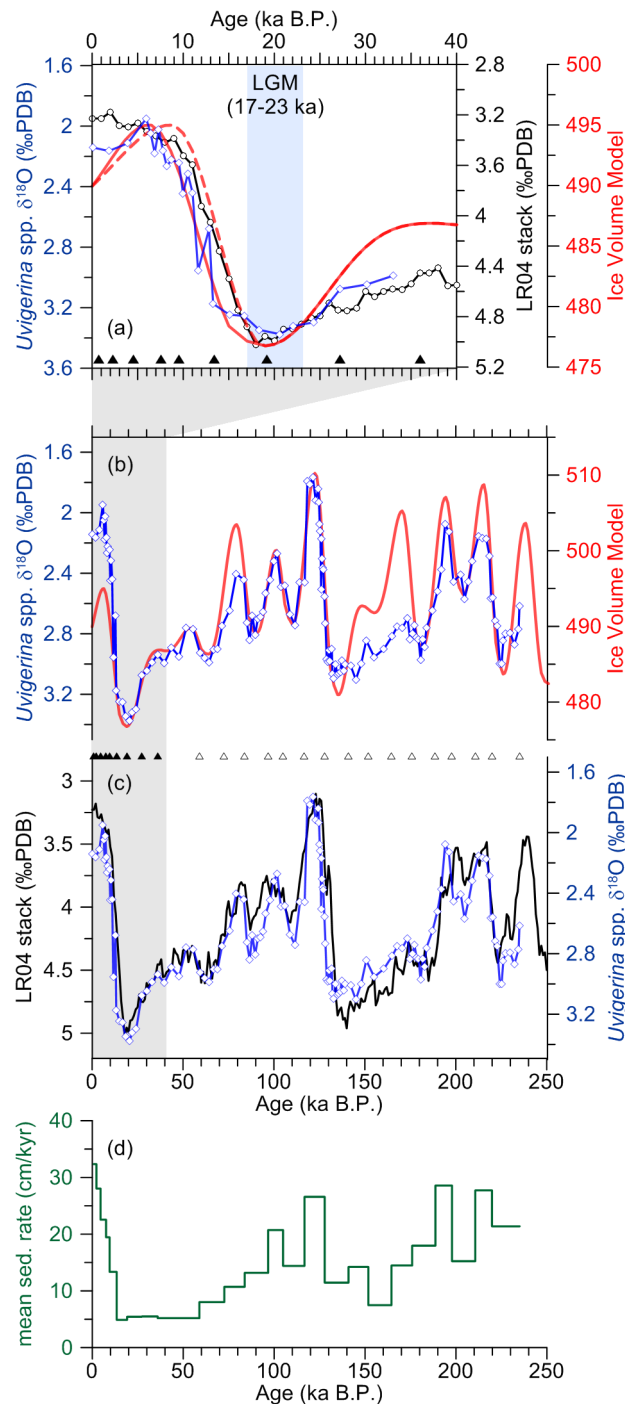


Figure 2. The age model of core MD10–3340, established on *Uvigerina* spp. $\delta^{18}\text{O}$ (blue), the LR04 benthic stack [Lisiecki and Raymo, 2005] (black), and the insolation-forced ice volume model [Imbrie and Imbrie, 1980] (red). Dashed and solid red lines denote the original and the 2/2.5 kyr lagged ice volume models, respectively. (a) 0–40 ka B.P., (b, c) 0–250 ka B.P., solid and open triangles show AMS ^{14}C and $\delta^{18}\text{O}$ correlated age controls, respectively. (d) mean sedimentation rate (green).

benthic $\delta^{18}\text{O}$ lagged the ice volume change by ~ 2 kyr, (3) the Holocene minimum in benthic $\delta^{18}\text{O}$ appeared ~ 2.5 kyr later than the ice-volume minimum. Accordingly, an adjusted ice volume model was generated by adjusting the original ice volume model with a ~ 2 kyr lag for the deglacial/warming intervals and ~ 2.5 kyr lag for the peak warm substages. The complete benthic $\delta^{18}\text{O}$ record of MD10–3340 was then tuned to this

calibration [Fairbanks et al., 2005] (supporting information Table S1). Because of the abundant existence of the coccolith *Emiliani huxleyi* (first occurrence at 270 ka B.P. [Thierstein et al., 1977]) throughout the record of MD10–3340, the bottom age of MD10–3340 can be no older than MIS7 and thus was defined by $\delta^{18}\text{O}$ records comparison (Figure 2) to be around the boundary between MIS7.4 and 7.5.

The traditional method to establish age models for marine records is to correlate the foraminifera $\delta^{18}\text{O}$ in one core with a standard $\delta^{18}\text{O}$ curve such as SPECMAP [Imbrie et al., 1984] or the LR04 benthic stack [Lisiecki and Raymo, 2005]. However, questions have arisen recently about the assumed global synchronicity underlying such approaches, in which benthic $\delta^{18}\text{O}$ was thought to be dominantly an indicator of global ice-volume or sea-level [Skinner and Shackleton, 2005, 2006]. To address such problems and acquire reliable age control on the precessional cycles, we established the age model of MD10–3340 on the basis of findings from the AMS ^{14}C dated section and by correlating the benthic (*Uvigerina* spp.) $\delta^{18}\text{O}$ record to the insolation forced nonlinear ice volume model of Imbrie and Imbrie [1980] rather than any stacked $\delta^{18}\text{O}$ record.

The ice volume model is defined by Imbrie and Imbrie [1980] as a function of the 65°N June 21st insolation [Laskar et al., 2004] (thus lower value represents higher ice volume), using the coefficients for the last 1.5 Ma (nonlinearity $b=0.6$, time constant $T_m=15$ kyr) of Lisiecki and Raymo [2005]. Comparison between the ^{14}C dated record of benthic $\delta^{18}\text{O}$ (0–40 ka) in MD10–3340 and the ice volume model (Figure 2a) reveals that: (1) the timing of the benthic $\delta^{18}\text{O}$ maximum appears synchronous with the ice-volume maximum, (2) the deglacial decreases of

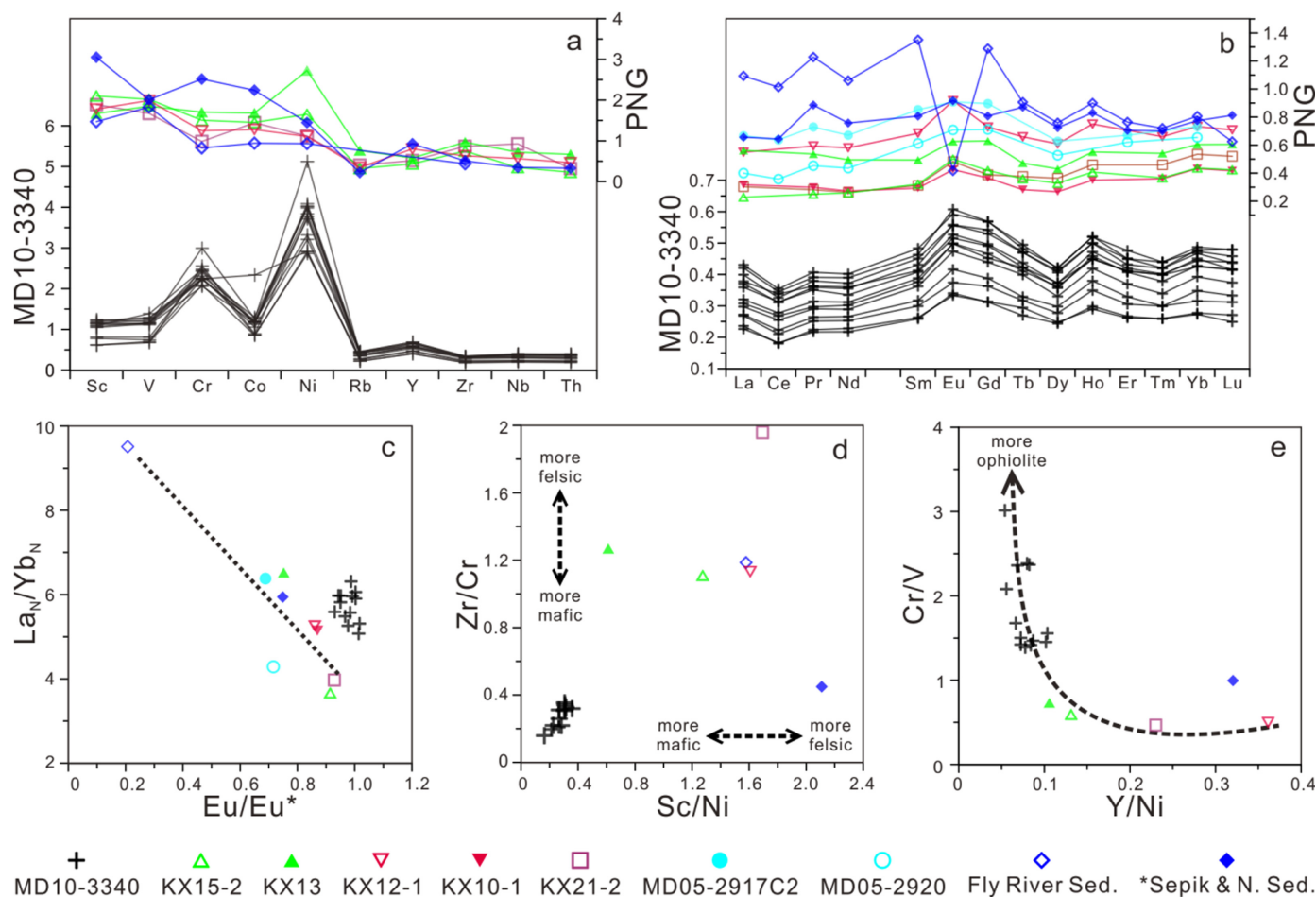


Figure 3. Trace and rare earth elements distributions and ratios in core MD10-3340 and PNG-derived sediment. (a) selected trace elements, and (b) REE, both normalized to Upper Continent Crust (UCC); (c) La_N/Yb_N versus Eu/Eu^* (chondrite normalized), linear correlation among PNG-derived sediments shown in dashed line; (d) Zr/Cr versus Sc/Ni ; (e) Cr/V versus Y/Ni . Symbols for sites are shown at the bottom. Data sources refer to supporting information Table S2.

adjusted ice volume model, assuming these time lags are coherent all along the core (Figure 2, supporting information Table S1). The resultant age model leads to a total phase lag of ~ 0.7 kyr of our *Uvigerina* spp. $\delta^{18}O$ record relative to the LR04 benthic stack in the precession band.

According to our age model, the last occurrence of *G. ruber* pink was found at the interval around 121.4 ka (1400–1401 cm core depth), in good agreement with the biostratigraphy datum given by Thompson *et al.* [1979]. The averaged mean sedimentation rate (MSR) downcore is ~ 14.4 cm/ka, with generally higher MSRs in interglacial stages ($\sim 20.8 \pm 7.0$ cm/ka) and warmer substages, and lower in glacial stages ($\sim 8.9 \pm 3.9$ cm/ka) and colder substages (Figure 2d). The large apparent decrease in core sedimentation rate over the interval from the core-top to ~ 13 ka may be caused by core stretching, a well-known phenomenon with the Calypso corer [Széréméta *et al.*, 2004].

4.2. Trace Element Characteristics

Trace element compositions are used to constrain the source of terrigenous sediment in core MD10-3340 since trace elemental geochemistry can faithfully reflect the characteristics of sediment provenance with little influence from sedimentation processes [e.g., McLennan *et al.*, 1993; Potter *et al.*, 2005]. The selected trace element and REE distribution patterns from all Marine Isotope Stages in MD10-3340 display consistent features (Figure 3, supporting information Table S2), including: (1) enrichments in elements from Sc to Co over those from Rb to Th, with very strong enrichments in Cr and Ni; (2) enrichment in major middle REEs (Sm, Eu, Gd, and Tb), and (3) a prominent positive Eu anomaly, $Eu/Eu^* \approx 1.0$ (0.98 ± 0.03 , 1σ) (UCC normalized).

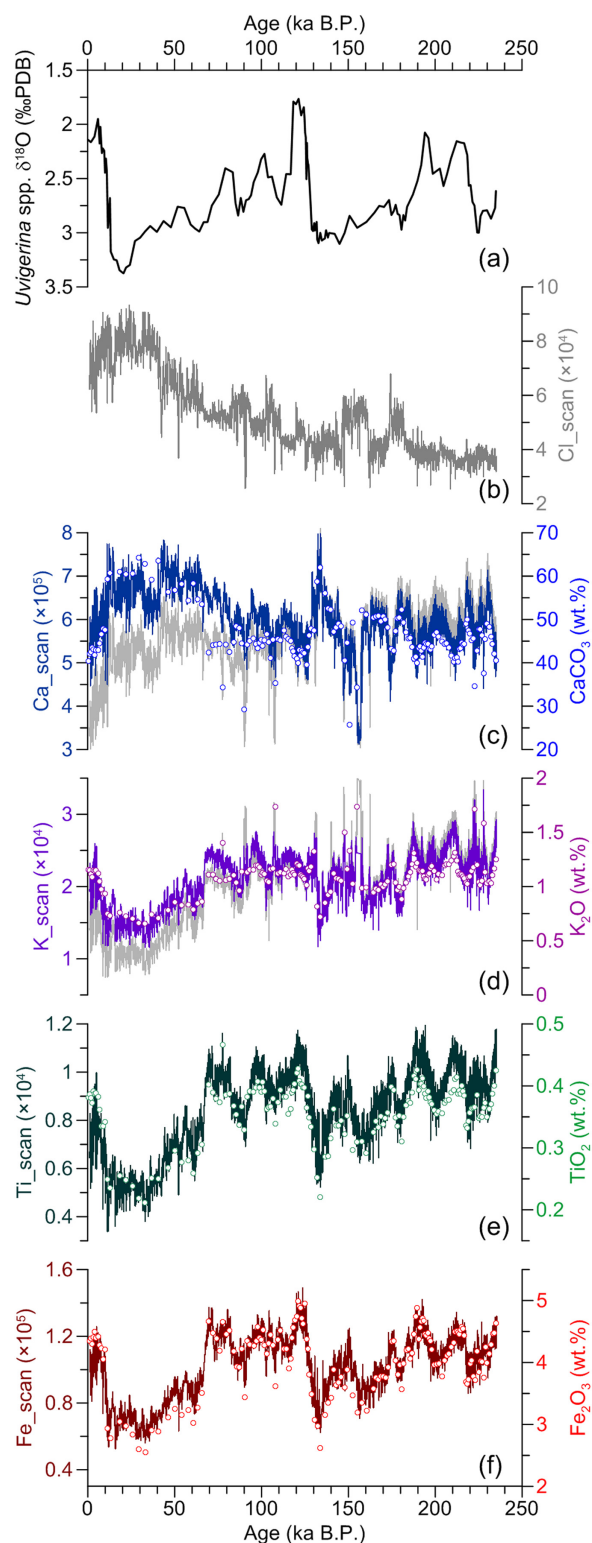


Figure 4. Major element compositions of MD10-3340 sediments measured by XRF (symbols) and core-scanning (thin lines). (a) *Uvigerina* spp. $\delta^{18}\text{O}$. (b) Cl_{scan} . (c, d) raw scanning (gray) and CI-corrected results of Ca and K. (e, f) Ti, and Fe.

Superimposed on the longer-term glacial-interglacial cycles, changes at higher frequencies are visible with high amplitude and stable periodicity. These can be more clearly seen in the scanning results because of the higher sampling resolution (Figure 4). Spectral analysis using Redfit38 [Schulz and Mudelsee, 2002] on the scanning XRF results

4.3. Major Element Compositions

The quantitative XRF measurements of major elements showed consistent patterns with respect to the scanned results (Figure 4), while apparent patterns associated with glacial-interglacial cycles can be seen in the major element compositions. The CaCO_3 concentration (mainly pelagic carbonate) is apparently higher by ~ 7 wt% in the intervals of MIS2-4 and MIS6 than those of MIS1, 5, and 7. The relative concentrations of Al_2O_3 , K_2O , TiO_2 , and Fe_2O_3 show identical variations opposite to those of CaCO_3 (Figure 4). In other words, increased (decreased) pelagic and decreased (increased) terrigenous fractions were deposited during Glacial (Interglacial) periods, which is in agreement with the lower (higher) mean sedimentation rate in Glacials (Interglacials) (Figure 2).

However, the scanning results show certain deviations from the XRF measured results, particularly in the lighter elements (K and Ca). These deviations are characterized by significant weakening of scanning intensities in the upper ~ 500 cm and glacial intervals as well as the gradual down-core increases in their scanning intensities. It is obvious that these scanning deviations are related to the scanned intensity of Cl (Figure 4), a monitor of the water content of the sediment. Higher Cl intensity indicates higher sea water content. The water content in cores can produce a strong attenuation effect on the XRF scanning results [Tjallingii et al., 2007; Henekam and de Lange, 2012], especially for lighter elements (K and Ca) as compared to heavier elements (Ti and Fe). For example, the differences between the median-value normalized Ca_{scan} and $\text{CaCO}_3_{\text{XRF}}$ [Lyle and Backman, 2013] show a strong correlation to the Cl_{scan} (supporting information Figure S1). Therefore, to correct the attenuation effect, we eliminated the anomalous changes related to the Cl_{scan} data from the original XRF scanning results [Henekam and de Lange, 2012]. The corrected results display much more reasonable agreement with their quantitative measurements (Figure 4).

Superimposed on the longer-term glacial-interglacial cycles, changes at higher frequencies are visible with high amplitude and stable periodicity. These can be more clearly seen in the scanning results because of the higher sampling resolution (Figure 4). Spectral analysis using Redfit38 [Schulz and Mudelsee, 2002] on the scanning XRF results

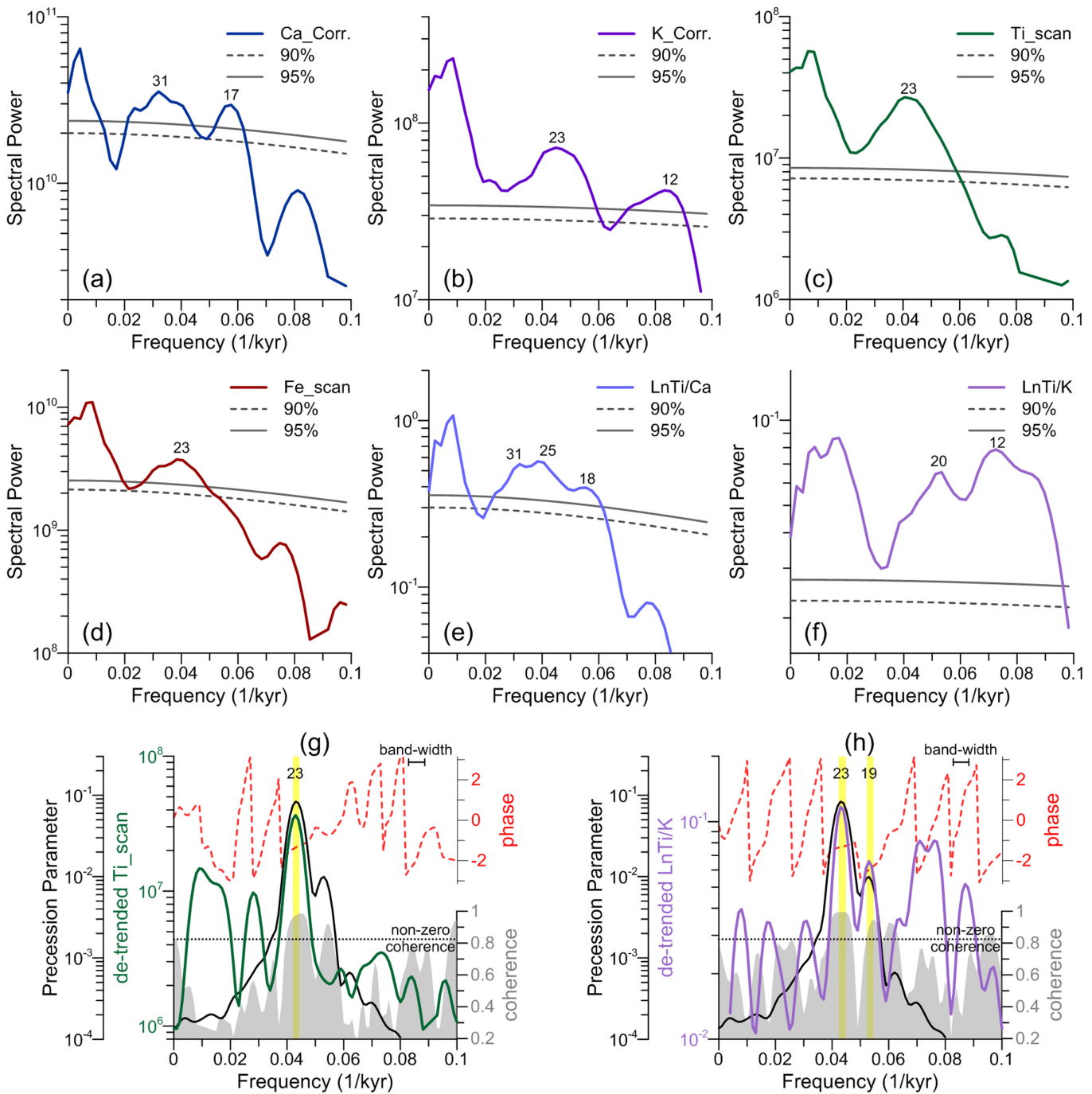


Figure 5. (a–f) Results of spectral analysis calculated on Ca_Corr., K_Corr., Ti_scan, Fe_scan, LnTi/Ca, LnTi/K using Redfit38 [Schulz and Mudelsee, 2002], gray lines denote 90% and 95% confidence level. (g, h) Phase-cross spectral analysis on detrended Ti_scan and LnTi/K with respect to precession parameter using Analyseries2.0.4.2 [Paillard et al., 1996], bandwidth=0.006, nonzero coherence>0.824.

show: (1) dominant periods of Ca_corr. at ~31 and ~17 ka; (2) dominant periods of the detrital elements at ~23 kyr, and a minor peak of K_corr. around ~12 kyr; (3) several peaks in periodicity of LnTi/Ca between 30 and 20 kyr; (4) two peak periods of LnTi/K at ~20 kyr and ~12 kyr (Figure 5). These periodicities in scanning results are in good agreement with those of XRF measurements (not shown).

To better distinguish the higher-frequency variations, the apparent glacial-interglacial trends in the scanning results were removed by subtracting the first principal component (PC1) calculated by singular

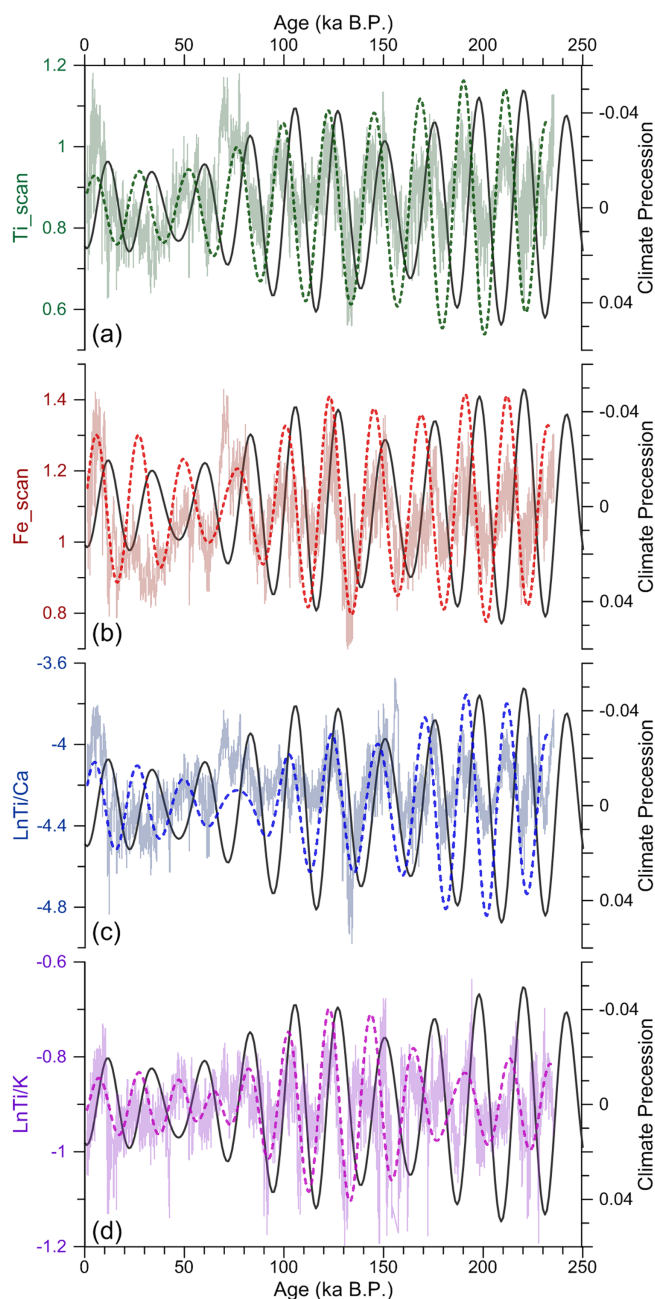


Figure 6. The detrended records (thin lines) and Gaussian-filtering (dotted lines) of terrigenous sediment proxies in core MD10-3340. (a–d) Ti_scan (green), Fe_scan (red), $Ln(Ti/Ca)$ (blue), and $Ln(Ti/K)$ (purple), respectively. Climatic precession parameter shown in thick black line.

ultra-mafic rocks like ophiolites [Potter et al., 2005]. In addition, the Eu/Eu^* values which generally equalize to 1, are solid evidence of young undifferentiated mantle-sourced island arc basalts [McLennan et al., 1993]. Accordingly, the terrigenous sediments in core MD10-3340 are inferred to be mainly sourced from basaltic to ultra-basaltic terranes, most likely from nearby Halmahera Island which was created by the collision of oceanic slabs [Hall et al., 1988, 1991; Ballantyne, 1991]. The uniform down-core REE composition supports a relatively homogeneous and solitary provenance of terrigenous sediment in MD10-3340 over glacial and interglacial periods.

Trace elemental compositions can further be compared between MD10-3340 and PNG-derived sediments, because Papua New Guinea (PNG) has previously been regarded as one major possible source of terrigenous sediment in the western tropical Pacific [e.g., Milliman, 1995] and thus also in the Halmahera Sea.

spectrum analyses (SSA of Analyseries2.0 [Paillard et al., 1996], with embedding dimensions taken as 1/10 of the number of data points, and using the method of Vautard and Ghil [1986]) (Figure 6). The detrended records of detrital elements and $LnTi/Ca$ and $LnTi/K$, as well as their 18~24 kyr band-pass Gaussian filtering (Analyseries2.0 [Paillard et al., 1996]) demonstrate constant phase relationships relative to the precession parameter [Laskar et al., 2004] (Figure 6). Results of cross-phase Blackman-Tukey analysis using a Tukey window (Analyseries2.0 [Paillard et al., 1996]) reveal phase lags between the maxima of Ti_scan and $LnTi/K$ ($\sim 103^\circ$, Figure 5), Fe_scan ($\sim 97^\circ$) and $LnTi/Ca$ ($\sim 86^\circ$) (not shown) and minima of the precession parameter. These findings can find further support from the results of the wavelet analysis of Ti_scan (supporting information Figure S2).

5. Discussions

5.1. Terrigenous Sediment Input As A Proxy of Local Precipitation

5.1.1. Provenance of the Terrigenous Sediments

The provenance of the terrigenous sediments in core MD10-3340 can be inferred from their trace elemental characteristics, including: (1) enrichment in trace elements from Sc to Ni; (2) strongly concentrated Cr and Ni; (3) the Eu signature. Sc, V, Co, Cr and Ni are typically enriched in mafic igneous rocks while Th, Nb, Zr, Y and Rb are more abundant in felsic materials [e.g., McLennan et al., 1993]. Cr and Ni preferentially occur in typical

However, significant differences can be observed between the two. In contrast with core MD10-3440, PNG-derived sediments show little or only minor enrichment in Cr and Ni (Figure 3a) and a reduced (e.g., Fly River) Eu anomaly (Figures 3b and 3c) (data sources see supporting information Table S2). Furthermore, Eu/Eu* in PNG-derived sediment ranges between 0.7 and 0.9 (0.85 ± 0.08 , 1σ , Fly River excluded) while it is around 1 in core MD10-3440 (Figure 3c). This shows the influence of intracontinental differentiation and/or mixing with continental materials on PNG sediments, and allows us to distinguish between the different island arc petrologic environments of PNG and Halmahera [McLennan *et al.*, 1993]. Also, data points from MD10-3340 fall outside the linear relationship between La_N/Yb_N and Eu/Eu* defined for the PNG-derived sediments ($R^2=0.91$ if Fly River included, $R^2=0.88$ if Fly River excluded) (Figure 3c). This supports a non-PNG provenance for the terrigenous sediment in core MD10-3340. Finally, ratios of ultra-mafic (Cr and Ni) to felsic (Zr) and to mafic (Sc, V, Y) elements [McLennan *et al.*, 1993] demonstrate significant differences between MD10-3340 and PNG-derived sediment, with much more enriched ultramafic contributions in MD10-3340 (Figures 3d and 3e). Thus, in contrast to the Halmahera region, the PNG-derived sediments contain more felsic materials, indicating sources from the intermediate-basaltic basement rock-type of PNG which is a marginal cordillera of the Australian continent [Davies, 2012; Wu *et al.*, 2013].

Therefore, we argue that the terrigenous fraction in MD10-3340 originates mainly from local riverine drainages from islands of the Halmahera region with limited exotic input. Variations in the relative content of terrigenous sediment in MD10-3340 are thus dominantly controlled by local terrigenous input. Considering the small island and the narrow shelf and basin of Halmahera, the influence of transport is assumed to be negligible for the terrigenous input into the sea. Hence, the terrigenous input into the Halmahera Sea can be tightly linked to local riverine discharge and hence local precipitation of the Halmahera region.

5.1.2. Proxies of Terrigenous Input

In the record of MD10-3340, variations in the contents of Al, K, Ti and Fe, as well as their ratios relative to Ca and the ratios of Ti/K, are generally similar (Figure 6). These elements are exclusively associated with terrigenous constituents, especially Ti and Fe, which are preferentially fed by basaltic rocks [e.g., Kissel *et al.*, 2010]. Due to the mafic source of terrigenous sediments in MD10-3340, we tend to use the contents of Ti and Fe as indicators for changes in input of the terrigenous sediment fraction, though care must be taken to avoid oversimplistic interpretations.

In marine sediment, Ca is dominantly associated with pelagic carbonate and Al is usually thought to be a constant major constituent of aluminosilicates; Ti is concentrated in heavy minerals (e.g., ilmenite, rutile and zirconium) and in coarser silt and sand fractions [e.g., Schmitz, 1987; Shimmiel and Mowbray, 1991]. Accordingly, Ti/Ca and Ti/Al ratios are usually taken to indicate the relative contributions of detrital versus pelagic, and silt/sand versus clay fractions in marine sediments, respectively [e.g., Kissel *et al.*, 2010; Lückge *et al.*, 2009].

However, in the equatorial Pacific, the biogenic scavenging of settling particles contributes significantly to sedimentary Al content [Murray and Leinen, 1996]. The Al contents of different types of aluminosilicate minerals can also vary widely, so using Al for normalization may be further biased by changes of aluminosilicates [e.g., Schneider *et al.*, 1997]. On the other hand, K in marine sediment occurs principally in the finer pelagic clay fraction, concentrating in phillipsite, K-mica and K-feldspar, and illite [Goldberg and Arrhenius, 1958; Weaver, 1967; Othman *et al.*, 1989; Schneider *et al.*, 1997]. Thus, we tend to use K instead of Al for the normalization of Ti (or Fe) in this study, to indicate the ratios of coarser heavier minerals.

Therefore, in this study, the concentrations of Ti and Fe serve as proxies for the terrigenous content of the sediments, and the Ti/Ca and Ti/K ratios for the contributions of detrital relative to pelagic fractions, and of heavier minerals relative to clay minerals, respectively. Variations in Ti and Fe contents and in $\ln(Ti/Ca)$ are highly consistent (Figure 6), although the spectral signature of $\ln(Ti/Ca)$ mixes the distinct signals of Ti_{scan} and Ca_{scan} (Figure 5). Variations in $\ln(Ti/K)$ are also consistent with Ti and Fe contents (Figure 6), while an additional ~ 12 kyr cycle is revealed by $\ln(Ti/K)$ (Figure 5). The consistency among these proxies suggests that Ti and Fe in MD10-3340 reliably indicate the terrigenous input, whereas $\ln(Ti/K)$ may provide further information about the variations of local terrigenous input on orbital time scales.

5.2. Orbital-Scale Variations in the Terrigenous Input

5.2.1. The Apparent Glacial-Cycle and the 30 kyr Period of Ca

The apparent glacial-cycle changes in the sedimentary records of MD10-3340, which are demonstrated by increased (decreased) sedimentation rates accompanied by higher (lower) concentrations of terrigenous

fractions during interglacial (glacial) intervals (Figures 2 and 4), might reflect enhanced (declined) terrigenous input during interglacial (glacial) times. Previous studies have shown that due to the cooling of SST and the exposure of the Sunda Shelf during Last Glacial, precipitation over the maritime Southeast Asia would be depressed as a result of the depression and/or eastward movement of the convective activity over IPWP [e.g., *DiNezio and Tierney, 2013*]. But, in our case, the apparent glacial-cycle changes in MD10-3340 may be complicated by influences induced from sea-level changes.

It is noteworthy that the relative increases of terrigenous sediments during interglacial intervals (decreases during glacial) in MD10-3340 is in contrast to the general view that terrigenous input increases during sea-level low-stands of glacial periods because of increased shelf exposure and decreased distance of river mouths to the sedimentary basin. Therefore, alternative processes might be involved. Firstly, one important line of evidence is that in contrast to MD10-3340, another core retrieved from deeper in the Halmahera basin (MD10-3339, 0.5°S, 128.8°E, ~1700 m water depth) shows relatively constant sedimentation rates from MIS4 to Holocene (~60 cm/ka) and only minor glacial-interglacial changes in the content of sediment fractions [Gustiantini et al., in preparation]. Thus, the apparent glacial cycles observed in the sediment composition of the shallower MD10-3340 might be complicated by sea-level-change related processes, like intrabasin sediment redistribution (winnowing and/or settling) possibly linked to sea-level controlled changes in bottom currents [van Aken et al., 1988]. Alternatively, changes in the relative contribution of carbonate production and changing distance from river mouths could also influence the variability of terrigenous fraction in our records. Further work is needed to better address this issue.

In addition, the amplitude of changes in the terrigenous input records of MD10-3340 is obviously suppressed in the last glacial period, particularly between 40 and 20 ka (Figures 6, and supporting information Figure S2). This might be a result of the attenuation effect of the extremely high water content in the Last Glacial sections (Figure 4b), or due to the lower concentration of the terrigenous fraction and smaller variations (Figure 4). But more likely, the reduced signal may be related to the smaller amplitude of changes in the precession band and hence insolation from MIS4 to MIS2.

The ~31 and ~17 kyr periods observed in the Ca content (Figure 5a), which mostly consists of the pelagic carbonate, is comparable to the ~30 and ~19 kyr periods of variations found in primary productivity records in the equatorial Pacific [e.g., *Beaufort et al., 2001*]. But these cycles in the Ca content is significantly different from the ~23 kyr cycles in the terrigenous elements (Figures 5c and 5d), and hence the possible dilution effect of carbonate fraction on terrigenous contents is suggested to be minor on the precessional band. While, the spectral peaks from ~18 to ~31 kyr in Ln(Ti/Ca) (Figure 5e) are obviously mixed signals stemmed from the combination of both terrigenous and carbonate fractions.

5.2.2. The Precessional Variations in Terrigenous Input

The dominant ~23 kyr period of the contents of Ti, Fe and the ~20 kyr period of Ln(Ti/K) (Figure 5) are interpreted as precessional cycle signals, while the ~12 kyr period observed in the Ln(Ti/K) approximates a half of the precession cycle. Precession-dominated variation in the terrigenous input and rainfall in our records is consistent with previous reports of regional terrigenous input [*Lückge et al., 2009; Kissel et al., 2010; Tachikawa et al., 2011; Wu et al., 2013*], speleothem $\delta^{18}\text{O}$ records [*Partin et al., 2007; Carolin et al., 2013*] (further discussed in sections 5.2.3 and 5.2.4) and Holocene leaf-wax δD [*Tierney et al., 2012*] from the IPWP.

The 90°~100° phase lag of the maximum terrigenous input in core MD10-3340 relative to the precession minimum (Figures 5 and 6), suggests that the precessional precipitation changes over Halmahera lag the June 21st insolation change by ~6 kyr, or in-phase correlates to the September–October insolation change. The reliability of this phase estimate is supported by our age model, which was established on the basis of benthic $\delta^{18}\text{O}$ record constrained by AMS ^{14}C dates and has already eliminated the possible timing differences underlying Pacific benthic $\delta^{18}\text{O}$, in spite of the 3–5 kyr uncertainty of the benthic $\delta^{18}\text{O}$ chronostratigraphy [*Skinner and Shackleton, 2006*]. We note that the phase lag of the terrigenous input relative to precession would still be around 90° if the age model was established by direct correlation of our benthic $\delta^{18}\text{O}$ record to the LR04 stack (not shown).

5.2.3. Possible ENSO-Related Forcing on the Precessional Hydroclimate Change Over the WEP

The precession-band variations in the terrigenous input in MD10-3340, and hence the precipitation over Halmahera which is in-phase with September–October insolation change, are in good agreement with the speleothem $\delta^{18}\text{O}$ records from northern Borneo [*Partin et al., 2007; Carolin et al., 2013*] (Figure 7, see Figure 1 for

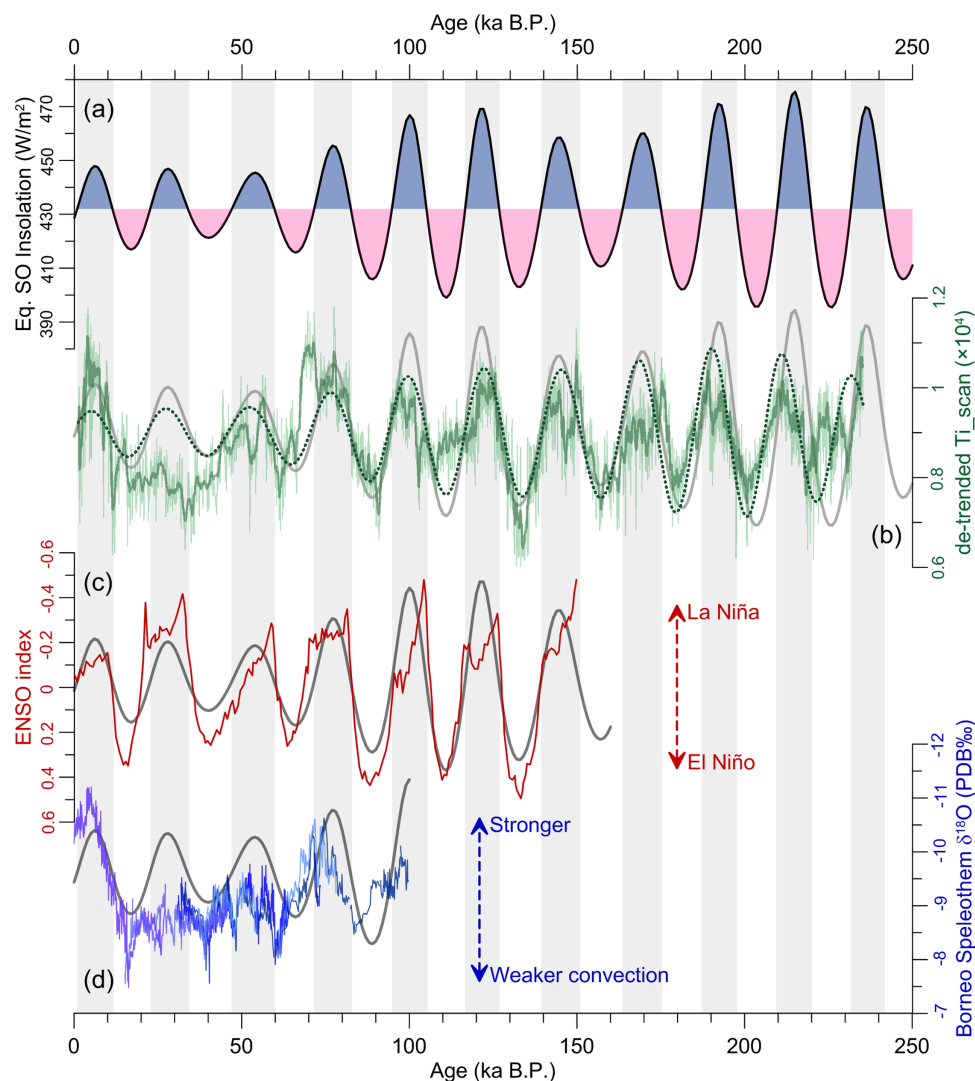


Figure 7. Precessional variations in hydroclimate of the western equatorial Pacific. (a) September–October insolation change at the Equator [Laskar *et al.*, 2004]. (b) detrended Ti_scan in MD10–3340. (c) ENSO index of Clement and Cane [1999]. (d) $\delta^{18}O$ of Northern Borneo speleothem [Partin *et al.*, 2007; Carolin *et al.*, 2013]. September–October insolation at the Equator is shown as gray lines in Figures 7b–7d.

site locations). A strong control of the seasonal rainfall during the months centered on September on the annual mean local precipitation of the Halmahera region is also observed in the modern climate (Figure 1c).

The significance of the boreal autumn season for the hydroclimate of the Halmahera region mainly comes from the interannual oscillations associated with ENSO [Hamada *et al.*, 2002; Aldrian and Susanto, 2003; Chang *et al.*, 2005; Aldrian *et al.*, 2007]. Due to the eastward displacement of the convective ascending branch of the Walker cell from maritime Southeast Asia towards the dateline during El Niño events [e.g., Philander, 1983], the local rainfall over Halmahera is greatly dampened during El Niño events. In contrast, La Niña events enhance the W–E SST gradient across the equatorial Pacific and strengthen the atmospheric convection and rainfall over the WEP (Figure 1c). Accordingly, a potential first order mechanism to explain the in-phase September–October insolation forcing on precipitation changes over Halmahera would be changes in the behavior of the ENSO system in the past.

Numerous studies have shown that during boreal late summer to early autumn, the ITCZ moves northward in the eastern equatorial Pacific (EEP), thus generating a divergent wind field in the east while the wind field remains convergent in the western Pacific. This late-summer zonal asymmetric wind-field pattern is thought to be a primary driving force for the development of ENSO [e.g., Rasmusson and Carpenter, 1982; Philander, 1983; Tziperman *et al.*, 1997; Clement and Cane, 1999; Clement *et al.*, 1999]. On orbital time scales, anomalous

heating due to an insolation increase in September would enhance the zonal asymmetry and the easterly wind anomaly, and it would amplify this perturbation via the same dynamics that give rise to ENSO, resulting in La Niña-like conditions. An anomalous cooling when insolation decreased, in contrast, would favor El Niño-like conditions [Clement and Cane, 1999; Clement et al., 1999].

Such an explanation finds support from the consistency between the simulated ENSO index of Clement and Cane [1999] and the paleorecords of terrigenous input at MD10-3340 and of Borneo speleothem $\delta^{18}\text{O}$ [Partin et al., 2007; Carolin et al., 2013] (Figure 7). Intervals of enhanced autumn insolation heating coincide with periods of enhanced precipitation over the equatorial western Pacific as indicated by increased terrigenous input in Halmahera Sea and more negative $\delta^{18}\text{O}$ in northern Borneo speleothem (Figure 7).

Modern observations demonstrate that rainfall $\delta^{18}\text{O}$ in northern Borneo shows lighter values in late boreal summer and heavier values in late winter, as well as strong positive anomalies in El Niño and negative anomalies in La Niña events [Cobb et al., 2007; Moerman et al., 2013]. The $\delta^{18}\text{O}$ values of northern Borneo stalagmites are interpreted as records of paleoprecipitation that are sensitive to the position and strength of the atmosphere convective activity over the equatorial western Pacific [Cobb et al., 2007; Partin et al., 2007; Carolin et al., 2013].

In addition, in accordance with the autumn insolation change, the Holocene maximum in the terrigenous input of MD10-3340 appears around 5 ka, which coincides with the minimum in $\delta^{18}\text{O}$ of northern Borneo stalagmites [Partin et al., 2007]. These records indicate increased convective activity and rainfall over the western equatorial Pacific during the Mid-Holocene relative to the Late and Early Holocene. Additionally, the zonal SST gradient across the equatorial Pacific reached a maximum and the variance of the EEP SST was lowest in the Mid-Holocene [Koutavas and Joanides, 2012]. Taken together, these findings point to scenarios of either a La Niña-like mean state or more La Niña than El Niño events in the Mid-Holocene, which can also find support from both paleorecord [e.g., Moy et al., 2002; Conroy et al., 2008] and model-simulation [e.g., Clement et al., 2000; Luan et al., 2012] results.

Therefore, it seems reasonable to draw the conclusion that the precessional variations in the hydroclimate of the equatorial western Pacific region are in-phase correlated to September–October insolation changes. A leading possible driving mechanism may be associated with the ENSO-like dynamics which regulate and control the atmosphere convective activity and hence precipitation over the WEP.

5.2.4. Role of Rainfall Seasonality on the Precessional Hydroclimate Change of WEP

In general, the modern seasonality of precipitation is weak over the Halmahera region as well as at the site of the northern Borneo stalagmite records [Aldrian and Susanto, 2003; Cobb et al., 2007]. Most gauge sites on Halmahera display a wetter season in the first-half year, and only a few show rainfall peaks in June–July [Aldrian et al., 2003]. The reason for the higher seasonal rainfall from May to July on Halmahera Island is suggested to be tightly linked to enhanced atmospheric convection due to higher SST of the Halmahera and Molluca Seas, which is determined mainly by the transport of warmer surface water from the warm pool northeast off Irian Jaya by the Indonesian Throughflow (ITF) [Aldrian et al., 2003].

Hence, the key to resolving the forcing of seasonality lies in the past changes in regional SST. Over the glacial terminations, because of the combined influence of CO_2 rising, ice sheet melting and ocean circulation, timing differences of 2–3 kyr may exist between SST of the IPWP and boreal summer insolation [e.g., Lea et al., 2000; Stott et al., 2007; Shakun et al., 2012]. During the Holocene, when insolation dominates, the SST of the IPWP varied generally in-phase with boreal summer insolation [e.g., Stott et al., 2004; Linsley et al., 2010; Dang et al., 2012]. It should therefore be safe to infer that SST of the IPWP is mainly determined by the boreal summer insolation forced sensible heating.

Accordingly, if the seasonality was driving the precessional changes of rainfall over the WEP, then a phase lag larger than 6 kyr would be implied between the insolation forced sensible heating of the rainy season and the local hydroclimate response. However, such a large phase lag is obviously incompatible with the hypothesized in-phase forcing mechanism of insolation on tropical hydroclimate change, as supported by both proxy records [e.g., Wang et al., 2001, 2008; Liu et al., 2014] and model simulations [e.g., Kutzbach et al., 2008; Ziegler et al., 2010]. Such a hypothesis would lead to approximately in-phase relationships among local summer insolation, sensible heating, atmospheric convection, and hence precipitation.

Apparently, processes other than direct sensible heating are involved in the hydroclimatic feedbacks of the WEP to insolation forcing. To explain the isotopic depletion of Borneo stalagmites in the Mid-Holocene, the effect of JJA perihelion on the boreal autumn ocean-atmosphere coupled dynamics was suggested by *Tierney et al.* [2012], with emphasis on the zonal Walker Circulation across the tropical Indian Ocean. In the Pacific, a record of thermocline salinity from the east equatorial Pacific indicates stronger upwelling (i.e., sharper W-E gradient) when boreal summer insolation is higher [*Pena et al.*, 2008]. In contrast, records of Mg/Ca-SST from both the west and east equatorial Pacific show an increased zonal SST gradient in peak glacial and decreased gradients in peak interglacial times [*Lea et al.*, 2000]. Hence, uncertainties remain in the processes that link the incoming insolation forcing to the record of hydroclimate changes of the WEP. Whether originating from the Indian or the Pacific Ocean, it is acknowledged that changes in the strength and position of the ascending branch of the Walker Circulation play a key role in determining the hydroclimate of the WEP. More work is needed to better resolve the air-sea coupled responses of the WEP.

5.2.5. The Conceptual Interhemisphere ITCZ Displacement

Previous records of terrigenous input from the southern parts of maritime Southeast Asia commonly have shown in-phasing linkage to the austral summer (DJF) insolation (Figure 7e) [*Lückge et al.*, 2009; *Kissel et al.*, 2010; *Tachikawa et al.*, 2011; *Wu et al.*, 2013] (see Figure 1 for core locations). These records generally reflect forcing of the AISM, as they experience the wet season from November to March when the ITCZ lies overhead [e.g., *Moron et al.*, 2010]. The record of *Kissel et al.* [2010] (MD06–3067) is particularly noteworthy because it is from the northern Hemisphere but shows an anticorrelation with the EASM. These authors therefore observed at this latitude a contrast between precipitation rates on land (East Asia) and in the marine realm [*Kissel et al.*, 2010]. Their data from Mindanao may therefore also indicate that precipitation related to the AISM developed as far north as 6°N [*Hamada et al.*, 2002; *Aldrian and Susanto*, 2003].

The in-phase relation between AISM and DJF insolation, together with the in-phase relation between EASM and JJA insolation as recorded by Chinese stalagmites [*Wang et al.*, 2001, 2008; *Yuan et al.*, 2004; *Cheng et al.*, 2009; *Liu et al.*, 2014], convincingly support the conceptual framework of local summer insolation forcing on monsoonal rainfall and the interhemisphere antiphasing displacement of the ITCZ on the precessional band [e.g., *Kutzbach et al.*, 2008]. Precessional change in the hydroclimate of WEP, which is in-phase with the boreal autumn insolation, therefore fits well into the concept of displacement of the ITCZ. Moreover, our new record and the Borneo stalagmite records [*Partin et al.*, 2007; *Carolin et al.*, 2013] highlight the importance of the autumn rather than spring season, in the conceptual meridional movement of the ITCZ along with the maxima of seasonal insolation. This pattern might be related to the asymmetric annual cycle of EASM and AISM: the southward propagation of the ITCZ from Asia and Australia in boreal autumn is continuous; on the other hand, the northward movement of the ITCZ experiences a sudden transition in the boreal spring, and the ITCZ is confined south of 5°N from January to May [*Hung et al.*, 2004; *Chang et al.*, 2005].

Finally, the ~12 kyr cycle in our Ln(Ti/K) record most likely reflects the semiprecessional changes in WEP precipitation, related to the biannual crossing of the ITCZ over the equator. In addition, a lag of 1–4 kyr between the AISM and austral summer insolation [*Kissel et al.*, 2010; *Tachikawa et al.*, 2011] observed in these precipitation records over the IPWP might be explained by the influence of El Niño, including the delayed onset and shortening of duration and strengthening of intensity, on the AISM [*Moron et al.*, 2008, 2010; *Taschetto et al.*, 2009], if our interpretation for MD10–3340 and the Borneo stalagmite records [*Partin et al.*, 2007; *Carolin et al.*, 2013] is taken into account.

6. Conclusions

On the basis of the chronology established using radiocarbon dating and marine $\delta^{18}\text{O}$ stratigraphy, we analyzed the elemental composition of sediments in core MD10–3340 from the Halmahera Sea, Western Equatorial Pacific, and its variation over the last ~240 ka. This has led to the following conclusions.

1. On the basis of the trace element composition, the terrigenous sediment deposited in the Halmahera Basin is characterized by mafic to ultra-mafic materials, indicating a major provenance locally from Halmahera Island.
2. Apparent increases in pelagic calcium carbonate and decreases in lithogenic components are observed during the glacial periods, suggesting less terrigenous sediment was deposited in glacial at the core site of

MD10-3340. This may be primarily generated by hydroclimate changes of IPWP over glacial cycles, or possibly related to some sea-level derived changes in the intrabasin sediment distribution processes.

3. The terrigenous input into Halmahera Basin shows significant variations in the precession band which are in-phase with Equatorial September–October insolation change. We interpret these variations as due to changes in local atmospheric convective activity and precipitation predominantly associated with changes in ENSO-like oscillations, in light of the fact that modern precipitation over Halmahera is dominated by interannual fluctuations associated with ENSO. Our interpretation is supported by both numerical modeling and proxy reconstructions, and provides a high-quality continuous record of changes in the ENSO system from the western Pacific.

4. Through comparisons with published reconstructions of monsoonal precipitation from the vicinity in IPWP and East Asia, our results help to show that boreal autumn is more important than spring for the precessional interhemisphere displacement of the ITCZ. The impact of ENSO on the AISM on precessional time-scales might be more complicated than the simple drying effect previously speculated.

Acknowledgments

This study was supported by funding to Z. Jian from the Natural Science Foundation of China (NSFC91428310, 91028004, and 41023004), and implemented under the France-China framework of LIA-MONOCL (Laboratoire International Associé: MONsoon, Ocean, and CLimate). The authors gratefully thank the crew, the IPEV group, and the scientific party of the MD181 “MONOCIR” cruise for their shipboard assistance, the laboratory assistants at Tongji University for their help in the laboratory, and two anonymous reviewers and Andreas Lückge for their constructive comments. Data from this study are available in the “supplementary information” or from the corresponding author (hw dang@gmail.com).

References

- Adler, R. F., et al. (2003), The Version 2 global precipitation climatology project (GPCP) monthly precipitation analysis (1979–present), *J. Hydrometeorol.*, *4*, 1147–1167.
- Aldrian, E., and R. D. Susanto (2003), Identification of three dominant rainfall regions within Indonesia and their relationship to sea surface temperature, *Int. J. Climatol.*, *23*, 1435–1452.
- Aldrian, E., L. Dumenil-Gates, D. Jacob, R. Podzun, and D. Gunawan (2004), Long-term simulation of Indonesian rainfall with the MPI regional model, *Climate Dynamics*, *22*, 795–814, doi:10.1007/s00382-004-0418-9.
- Aldrian, E., L. Dumenil-Gates, and F. H. Widodo (2007), Seasonal variability of Indonesian rainfall in ECHAM4 simulations and in the reanalyses: The role of ENSO, *Theoretical and Applied Climatology*, *87*, 41–59.
- Ballantyne, P. (1991), Petrological constraints upon the provenance and genesis of the East Halmahera Ophiolite, *J. Southeast Asian Earth Sci.*, *6*, 259–269.
- Beaufort, L., T. d. Garidel-Thoron, A. C. Mix, and N. G. Pisias (2001), ENSO-like forcing on oceanic primary production during the late pleistocene, *Science*, *293*, 2440–2444.
- Beaufort, L., T. d. Garidel-Thoron, B. Linsley, D. Oppo, and N. Buchet (2003), Biomass burning and oceanic primary production estimates in the Sulu Sea area over the last 380 kyr and the East Asian monsoon dynamics, *Mar. Geol.*, *201*, 53–65.
- Butzin, M., M. Prange, and G. Lohmann (2005), Radiocarbon simulations for the glacial ocean: The effects of wind stress, Southern Ocean sea ice and Heinrich events, *Earth Planet. Sci. Lett.*, *235*, 45–61.
- Carolin, S. A., K. M. Cobb, J. F. Adkins, B. Clark, J. L. Conroy, S. Lejau, J. Malang, and A. A. Tuen (2013), Varied response of western Pacific hydrology to climate forcings over the last glacial period, *Science*, *340*, 1564–1566, doi: 10.1126/science.1233797.
- Chang, C.-P., Z. Wang, J. McBride, and C.-H. Liu (2005), Annual cycle of southeast Asia-maritime continent rainfall and the asymmetric monsoon transition, *J. Clim.*, *18*, 287–301.
- Cheng, X., B. Huang, Z. Jian, Q. Zhao, J. Tian, and J. Li (2005), Foraminiferal isotopic evidence for monsoonal activity in the South China Sea: a present-LGM comparison, *Marine Micropaleontology*, *54*(1–2), 125–139.
- Cheng, H., R. L. Edwards, W. S. Broecker, G. H. Denton, X. Kong, Y. Wang, R. Zhang, and X. Wang (2009), Ice age terminations, *Science*, *326*, 248–252, doi:10.1126/science.1177840.
- Clemens, S. C., and W. L. Prell (2007), The timing of orbital-scale Indian monsoon changes, *Quat. Sci. Rev.*, *26*, 275–278.
- Clement, A. C., and M. Cane (1999), A role for the tropical Pacific coupled ocean-atmosphere system on Milankovitch and millennial time-scales. Part I: A modeling study of tropical Pacific variability, in *Mechanisms of Global Climate Change at Millennial Time Scales*, *Geophys. Monogr. Ser.*, vol. 112, edited by P. U. Clark, R. S. Webb and L. D. Keiwin, pp. 363–371, AGU, Washington, D. C.
- Clement, A. C., R. Seager, and M. A. Cane (1999), Orbital control on the El Niño/Southern Oscillation and tropical climate, *Paleoceanography*, *14*, 441–456.
- Clement, A. C., R. Seager, and M. A. Cane (2000), Suppression of El Niño during the mid-Holocene by changes in the Earth’s orbit, *Paleoceanography*, *15*, 731–737.
- Clement, A. C., A. Hall, and A. J. Broccoli (2004), The importance of precessional signals in the tropical climate, *Clim. Dyn.*, *22*, 327–341.
- Cobb, K. M., J. F. Adkins, J. W. Partin, and B. Clark (2007), Regional-scale climate influences on temporal variations of rainwater and cave dripwater oxygen isotopes in northern Borneo, *Earth and Planetary Science Letters*, *263*, 207–220.
- Conroy J. L., J. T. Overpeck, J. E. Cole, T. M. Shanahan, and M. Steinitz-Kannan (2008), Holocene changes in eastern tropical Pacific climate inferred from a Galapagos lake sediment record, *Quat. Sci. Rev.*, *27*, 1166–1180.
- Cresswell, G. R., and J. L. Luick (2001), Current measurements in the Halmahera Sea, *J. Geophys. Res.*, *106*, 13,945–13,951.
- Cruz, F. W., S. J. Burns, I. Karmann, W. D. Sharp, M. Vuille, A. O. Cardoso, J. A. Ferrari, P. L. S. Dias, and O. Viana Jr. (2005), Insolation-driven changes in atmospheric circulation over the past 116,000 years in subtropical Brazil, *Nature*, *434*, 63–66.
- Dang H., Z. Jian, F. Bassinot, P. Qiao, and X. Cheng (2012), Decoupled Holocene variability in surface and thermocline water temperatures of the Indo-Pacific warm pool, *Geophys. Res. Lett.*, *39*, L01701, doi:10.1029/2011GL051054.
- Davies, H. L. (2012), The geology of New Guinea: The cordilleran margin of the Australian continent, *Episodes*, *35*, 87–102.
- Denniston, R. F., K.-H. Wyrwoll, V. J. Polyak, et al. (2013), A Stalagmite record of Holocene Indonesian-Australian summer monsoon variability from the Australian tropics, *Quaternary Science Reviews*, *78*, 155–168.
- DiNezio, P. N., and J. E. Tierney, (2013), The effect of sea level on glacial Indo-Pacific climate, *Nat. Geosci.*, *6*, 485–491, doi:10.1038/NGEO1823.
- Fairbanks, R. G., R. A. Mortlock, T.-C. Chiu, L. Cao, A. Kaplan, T. P. Guilderson, T. W. Fairbanks, A. L. Bloom, P. M. Grootes, and M.-J. Nadeau (2005), Radiocarbon calibration curve spanning 0 to 50,000 years BP based on paired ^{230}Th / ^{234}U / ^{238}U and ^{14}C dates on pristine corals, *Quat. Sci. Rev.*, *24*, 1781–1796.

- Godfrey, J. S. (1996), The effect of the Indonesian throughflow on ocean circulation and heat exchange with the atmosphere: A review, *J. Geophys. Res.*, *101*, 12,217–12,237.
- Goldberg E. D., and G. O. S. Arrhenius (1958), Chemistry of Pacific pelagic sediments, *Geochim. Cosmochim. Acta*, *13*, 153–212.
- Gordon, A. L. (2005), Oceanography of the Indonesian seas and its throughflow, *Oceanography*, *18*, 14–27.
- Griffiths, M. L., et al. (2009), Increasing Australian–Indonesian monsoon rainfall linked to early Holocene sea-level rise, *Nat. Geosci.*, *2*, doi:10.1038/NGEO605.
- Hakim, A. S., and R. Hall (1991), Tertiary volcanic rocks from the Halmahera Arc, Eastern Indonesia, *J. Southeast Asian Earth Sci.*, *6*, 271–287.
- Hall, R., G. Nichols, P. Ballantyne, T. Charlton and J. Ali (1991), The character and significance of basement rocks of the southern Molucca Sea region, *J. Southeast Asian Earth Sci.*, *6*, 249–258.
- Hamada, J.-I., M. D. Yamanaka, J. Matsumoto, S. Fukao, P. A. Winarso, and T. Sribimawati (2002), Spatial and temporal variations of the rainy season over Indonesia and their link to ENSO, *J. Meteorol. Soc. Jpn.*, *80*, 285–310.
- Haug, G. H., K. A. Huguen, D. M. Sigman, L. C. Peterson, and U. Röhl (2001), Southward Migration of the Intertropical Convergence Zone Through the Holocene, *Science*, *293*, 1304–1308.
- Hennekam, R., and G. d. Lange (2012), X-ray fluorescence core scanning of wet marine sediments: methods to improve quality and reproducibility of high resolution paleoenvironmental records, *Limnol. Oceanogr.*, *10*, 991–1003.
- Hettler, J., G. Irion, and B. Lehmann (1997), Environmental impact of mining waste disposal on a tropical lowland river system: A case study on the Ok Tedi Mine, Papua New Guinea, *Miner. Deposita*, *32*, 280–291.
- Hung, C.-W., X. Liu, and M. Yanai (2004), Symmetry and asymmetry of the Asian and Australian summer monsoons, *J. Clim.*, *17*, 2413–2426.
- Imbrie, J., and J. Z. Imbrie (1980), Modeling the climatic response to orbital variations, *Science*, *207*, 943–953.
- Imbrie, J., J. D. Hays, D. G. Martinson, A. McIntyre, A. C. Mix, J. J. Morley, N. G. Pisias, W. L. Prell, and N. J. Shackleton (1984), The orbital theory of Pleistocene climate: Support from a revised chronology of the marine $\delta^{18}\text{O}$ record, in *Milankovitch and Climate, Part 1*, NATO ASI Ser. C: Math. Phys. Sci., vol. 126, edited by A. Berger et al., pp. 269–306, D. Reidel Publishing Company, Dordrecht, Holland.
- Kershaw, A. P., S. C. Bretherton, and S. van der Kaars (2007), A complete pollen record of the last 230 ka from Lynch's Crater, north-eastern Australia, *Palaeogeogr. Palaeoclimatol. Palaeoecol.*, *251*, 23–45.
- Kissel, C., C. Laj, M. Kienast, T. Bolliet, A. Holbourn, P. Hill, W. Kuhnt, and P. Braconnot (2010), Monsoon variability and deep oceanic circulation in the western equatorial Pacific over the last climatic cycle: Insights from sedimentary magnetic properties and sortable silt, *Paleoceanography*, *25*, PA3215, doi:10.1029/2010PA001980.
- Koutavas, A., and S. Joannides (2012), El Niño–Southern oscillation extreme in the Holocene and last glacial maximum, *Paleoceanography*, *27*, PA4208, doi:10.1029/2012PA002378.
- Kutzbach, J. E., X. Liu, Z. Liu, and G. Chen (2008), Simulation of the evolutionary response of global summer monsoons to orbital forcing over the past 280,000 years, *Clim. Dyn.*, *30*, 567–579.
- Laskar, J., P. Robutel, F. Joutel, M. Gastineau, A. C. M. Correia, and B. Levrard (2004), A long-term numerical solution for the insolation quantities of the Earth, *Astronomy and Astrophysics*, *428*, 261–285.
- Lau, N.-C., and M. J. Nath (2000), Impact of ENSO on the variability of the Asian–Australian monsoons as simulated in GCM experiments, *J. Clim.*, *13*, 4287–4309.
- Lea, D. W., D. K. Pak, and H. J. Spero (2000), Climate impact of late Quaternary equatorial Pacific sea surface temperature variations, *Science*, *289*, 1719–1724.
- Linsley, B. K., Y. Rosenthal, and D. W. Oppo (2010), Holocene evolution of the Indonesian throughflow and the western Pacific warm pool, *Nat. Geosci.*, *3*, 578–583.
- Lisiecki, L. E., and M. E. Raymo (2005), A Pliocene–Pleistocene stack of 57 globally distributed benthic $\delta^{18}\text{O}$ records, *Paleoceanography*, *20*, PA1003, doi:10.1029/2004PA001071.
- Liu, Z., et al. (2014), Chinese cave records and the East Asia summer monsoon, *Quat. Sci. Rev.*, *83*, 115–128, doi:10.1016/j.quascirev.2013.10.1021.
- Luan, Y., P. Braconnot, Y. Yu, W. Zheng, and O. Marti (2012), Early and mid-Holocene climate in the tropical Pacific: Seasonal cycle and inter-annual variability induced by insolation changes, *Clim. Past Discuss.*, *8*, 505–555.
- Lückge, A., M. Mohtadi, C. Rühlemann, G. Scheeder, A. Vink, L. Reinhardt, and M. Wiedicke (2009), Monsoon versus ocean circulation controls on paleoenvironmental conditions off southern Sumatra during the past 300,000 years, *Paleoceanography*, *24*, PA1208, doi:10.1029/2008PA001627.
- Lyle, M., and J. Backman (2013), Data report: calibration of XRF-estimated CaCO_3 along the Site U1338 splice1, *Proc. Integrated Ocean Drill. Program*, *320/321*, 320205–322013 pp, doi:10.2204/iodp.proc.320321.
- McDonough, W. F., and S.-S. Sun (1995), The composition of the Earth, *Chem. Geol.*, *120*, 223–253.
- McLennan, S. M., S. Hemming, D. K. McDaniel, and G. N. Hanson (1993), Geochemical approaches to sedimentation, provenance, and tectonics. in *Processes Controlling the Composition of Clastic Sediments*, edited by M. J. Johnsson and A. Basu, pp. 21–40, Geol. Soc. Am. (spec. pap.), Boulder, Colo.
- Milliman, J. D. (1995), Sediment discharge to the ocean from small mountainous rivers: the New Guinea example, *Geo Mar. Lett.*, *15*, 127–133.
- Milliman, J. D., and K. L. Farnsworth (2011), *River discharge to the coastal ocean, a global synthesis*, pp. 45–46, Cambridge Univ. Press, Cambridge.
- Moerman, J. W., K. M. Cobb, J. F. Adkins, H. Sodemann, B. Clark, and A. A. Tuen (2013), Diurnal to interannual rainfall $\delta^{18}\text{O}$ variations in northern Borneo driven by regional hydrology, *Earth Planet. Sci. Lett.*, *369–370*, 108–119.
- Morey, S. L., J. F. Shriver, and J. J. O'Brien (1999), The effects of Halmahera on the Indonesian throughflow, *J. Geophys. Res.*, *104*, 23,281–23,296.
- Moron, V., A. W. Robertson, and R. Boer (2008), Spatial coherence and seasonal predictability of monsoon onset over Indonesia, *J. Clim.*, *22*, 840–850, doi:10.1175/2008JCLI2435.1171.
- Moron, V., A. W. Robertson, and J.-H. Qian (2010), Local versus regional-scale characteristics of monsoon onset and post-onset rainfall over Indonesia, *Clim. Dyn.*, *34*, 281–299, doi:10.1007/s00382-00009-00547-00382.
- Moy, C. M., G. O. Seltzer, D. T. Rodbell, and D. M. Anderson (2002), Variability of El Niño/Southern Oscillation activity at millennial timescales during the Holocene epoch, *Nature*, *420*, 162–166.
- Murray, R. W., and M. Leinen (1996), Scavenged excess aluminum and its relationship to bulk titanium in biogenic sediment from the central equatorial Pacific ocean, *Geochim. Cosmochim. Acta*, *60*, 3869–3878.
- Othman, D. B., W. M. White, and J. Patchett (1989), The geochemistry of marine sediments, island arc magma genesis, and crust–mantle recycling, *Earth Planet. Sci. Lett.*, *94*, 1–21.
- Paillard, D., L. Labeyrie, and P. Yiou (1996), Macintosh Program performs time-series analysis, *Eos Trans. AGU*, *77*, 379.

- Partin, J. W., K. L. Cobb, J. F. Adkins, B. Clarck, and D. P. Fernandez (2007), Millennial-scale trends in west Pacific warm pool hydrology since the Last Glacial Maximum, *Nature*, *449*, 452–456.
- Pena, L. D., I. Cacho, P. Ferretti, and M. A. Hall (2008), El Niño–Southern Oscillation–like variability during glacial terminations and interlatitudinal teleconnections, *Paleoceanography*, *23*, PA3101, doi:10.1029/2008PA001620.
- Philander, S. G. H. (1983), El Niño Southern Oscillation phenomena, *Nature*, *302*, 295–301, doi:10.1038/302295a302290.
- Potter, P. E., J. B. Maynard, and P. J. Depetris (2005), Provenance of mudstone, in *Mud and mudstone: Introduction and overview*, edited by P. E. Potter, J. B. Maynard, and P. J. Depetris, pp. 157–174, Springer, N. Y.
- Rasmusson, E. M., and T. H. Carpenter (1982), Variations in tropical sea surface temperature and surface wind fields associated with the Southern Oscillation/El Niño, *Mon. Weather Rev.* *110*, 354–384.
- Ruddiman, W. F. (2006), What is the timing of orbital-scale monsoon changes?, *Quat. Sci. Rev.*, *25*, 657–658.
- Schmitz, B. (1987), The TiO₂/Al₂O₃ ratio in the Cenozoic Bengal Abyssal Fan sediments and its use as a paleostream indicator, *Mar. Geol.*, *76*, 195–206.
- Schneider, R. R., B. Price, P. J. Müller, D. Kroon, and I. Alexander (1997), Monsoon related variations in Zaire (Congo) sediment load and influence of fluvial silicate supply on marine productivity in the east equatorial Atlantic during the last 200,000 years, *Paleoceanography*, *12*, 463–481.
- Schulz, M., and M. Mudelsee (2002), REDFIT: estimating red-noise spectra directly from unevenly spaced paleoclimatic time series, *Comput. Geosci.*, *28*, 421–426.
- Shakun, J., P. U. Clark, F. He, S. A. Marcott, A. C. Mix, Z. Liu, B. Otto-Bliesner, A. Schmittner, and E. Bard (2012), Global warming preceded by increasing carbon dioxide concentrations during the last deglaciation, *Nature*, *484*, 49–54, doi:10.1038/nature10915.
- Shimmield, G. B., and S. R. Mowbray (1991), The inorganic geochemical record of the northwest Arabian Sea: A history of productivity variation over the last 400 k.y. from Sites 722 and 724, *Proc. Ocean Drill. Program Sci.*, *117*, 409–429.
- Skinner L. C., and N. J. Shackleton (2005), An Atlantic lead over Pacific deep-water change across Termination 1: Implications for the application of the marine isotope stage stratigraphy, *Quat. Sci. Rev.*, *24*, 571–580.
- Skinner L. C., and N. J. Shackleton (2006), Deconstructing Terminations I and II: Revisiting the glacioeustatic paradigm based on deep-water temperature estimates, *Quat. Sci. Rev.*, *25*, 3312–3321.
- Stott, L., K. Cannariato, R. Thunell, G. H. Haug, A. Koutavas, and S. Lund (2004), Deline of surface temperature and salinity in the western tropical Pacific Ocean in the Holocene epoch, *Nature*, *431*, 56–59.
- Stott, L., A. Timmermann, and R. Thunell (2007), Southern hemisphere and deep-sea warming led deglacial atmosphere CO₂ rise and tropical warming, *Science*, *318*, 435–438, doi:10.1126/science.1143791.
- Szérémetá, N., F. Bassinot, Y. Balut, L. Labeyrie, and M. Pagel (2004), Oversampling of sedimentary series collected by giant piston corer: Evidence and correction based on 3.5-kHz chirp profiles, *Paleoceanography*, *19*, PA1005, doi: 10.1029/2002PA000795.
- Tachikawa, K., O. Cartapanis, L. Vidal, L. Beaufort, T. Barlyaeva, and E. Bard (2011), The precession phase of hydrological variability in the Western Pacific Warm Pool during the past 400 ka, *Quat. Sci. Rev.*, *30*, 3716–3727.
- Taschetto, A. S., C. C. Ummerhofer, A. S. Gupta, and M. H. England (2009), Effect of anomalous warming in the central Pacific on the Australian monsoon, *Geophys. Res. Lett.*, *36*, L12704, doi:10.1029/2009GL038416.
- Thierstein, H. R., K. R. Geitzenauer, B. Molfino, and N. J. Shackleton (1977), Global synchronicity of late Quaternary coccolith datum levels: Validation by oxygen isotopes, *Geology*, *5*, 400–404.
- Thompson, P. R., A. w. H. Bé, J.-C. Duplessy, and N. J. Shackleton (1979), Disappearance of pink-pigmented *Globigerinoides ruber* at 120,000 yr BP in the Indian and Pacific Oceans, *Nature*, *280*, 554–558.
- Tierney, J. E., D. W. Oppo, A. N. LeGrande, Y. Huang, Y. Rosenthal, and B. K. Linsley (2012), The influence of Indian Ocean atmospheric circulation on Warm Pool hydroclimate during the Holocene epoch, *J. Geophys. Res.*, *117*, D19108, doi:10.1029/2012JD018060.
- Tjallingii, R., U. Rohl, M. Kölling, and T. Bickert (2007), Influence of the water content on X-ray fluorescence coresampling measurements in soft marine sediments, *Geochem. Geophys. Geosyst.*, *8*, Q02004, doi:10.1029/2006GC001393.
- Tziperman, E., S. E. Zebiak, and M. A. Cane (1997), Mechanisms of seasonal-ENSO interaction, *J. Atmos. Sci.*, *54*, 61–71.
- van Aken, H. M. V., J. Punjawan, and S. Saimima (1988), Physical Aspects of the Flushing of the East Indonesian Basins, *Netherlands Journal of Sea Research*, *22*(4), 315–339.
- van der Kaars, W. A., and M. A. C. Dam (1995), 135,000-year record of vegetational and climatic change from the Bandung area, West-Java, Indonesia, *Palaeogeogr. Palaeoclimatol. Palaeoecol.*, *117*, 55–72.
- van der Kaars, S., P. D. Deckker, and F. X. Gingele (2006), A 100 000-year record of annual and seasonal rainfall and temperature for north-western Australia based on a pollen record obtained offshore, *J. Quat. Sci.*, *21*, 879–889.
- van der Kaars, S., N. Tapper, and E. J. Cook (2010), Observed relationships between El Niño–Southern Oscillation, rainfall variability and vegetation and fire history on Halmahera, Maluku, Indonesia, *Global Change Biol.*, *16*, doi:10.1111/j.1365-2486.2009.02025.x.
- Vautard, R., and M. Ghil (1989), Singular spectrum analysis in nonlinear dynamics, with applications to paleoclimatic time series, *Physica D*, *35*, 395–424.
- Wang, C. (2003), Atmospheric Circulation Cells Associated with the El Niño–Southern Oscillation, *Journal of Climate*, *15*, 399–419.
- Wang, X., A. S. Auler, R. L. Edwards, H. Cheng, E. Ito, Y. Wang, X. Kong, and M. Solheid (2007), Millennial-scale precipitation changes in southern Brazil over the past 90,000 years, *Geophys. Res. Lett.*, *34*, L23701, doi:10.1029/2007GL031149.
- Wang, Y. J., H. Cheng, R. L. Edwards, Z. S. An, J. Y. Wu, C. C. Shen, and J. A. Dorale (2001), A high-resolution absolute-dated late pleistocene monsoon record from Hulu Cave, China, *Science*, *294*, 2345–2348.
- Wang, Y., H. Cheng, R. L. Edwards, X. Kong, X. Shao, S. Chen, J. Wu, X. Jiang, X. Wang, and Z. An (2008), Millennial- and orbital-scale changes in the East Asian monsoon over the past 224,000 years, *Nature*, *451*, 1090–1093.
- Weaver, C. E. (1967), Potassium, illite and the ocean, *Geochim. Cosmochim. Acta*, *31*, 2181–2196.
- Wu, J., Z. Liu, and C. Zhou (2013), Provenance and supply of Fe-enriched terrigenous sediments in the western equatorial Pacific and their relation to precipitation variations during the late Quaternary, *Global Planet. Change*, *108*, 56–71.
- Wu, J. W., Z. F. Liu, and C. Zhou (2012), Late Quaternary glacial cycle and precessional period of clay mineral assemblages in the Western Pacific Warm Pool, *Chin. Sci. Bull.*, *57*, 1–13, doi: 10.1007/s11434-012-5277-x.
- Yuan, D., et al. (2004), Timing, duration, and transitions of the last interglacial Asian monsoon, *Science*, *304*, 575–578.
- Zhu, M., L. Stott, B. Buckley, K. Yoshimura, and K. Ra (2012), Indo-Pacific warm pool convection and ENSO since 1867 derived from Cambodian pine tree cellulose oxygen isotopes, *J. Geophys. Res.*, *117*, D11307, doi:10.1029/2011JD017198.
- Ziegler, M., L. J. Lourens, E. Tuenter, F. Hilgen, G.-J. Reichert, and N. Weber (2010), Precession phasing offset between Indian summer monsoon and Arabian Sea productivity linked to changes in overturning circulation, *Paleoceanography*, *25*, PA3213, doi:10.1029/2009PA001884.